Grain scale processes recorded by oxygen isotopes in olivine-hosted melt inclusions from two MORB samples

Mélina Manzini[1], Anne-Sophie Bouvier[1*], Lukas P. Baumgartner[1], Estelle F. Rose-Koga[2], Pierre Schiano[2], Nobumichi Shimizu[3]

[1] Institute of Earth Sciences, University of Lausanne, 1015 Lausanne, Switzerland

(melina.manzini@gmail.com; anne-sophie.bouvier@unil.ch; lukas.baumgartner@unil.ch)

[2] Laboratoire Magmas et Volcans, University of Blaise Pascal-CNRS-IRD, Clermont-Ferrand, France

(estelle.koga@uca.fr; p.schiano@opgc.fr)

[3] Woods Hole Oceanic Institution, Woods Hole, MA 02543, USA

(nshimizu@whoi.edu)

Corresponding author: A.-S. Bouvier (anne-sophie.bouvier@unil.ch)

Abstract

Although olivine-hosted melt inclusions from mid ocean ridge basalts (MORB) are commonly used as a proxy for mantle composition, these melt inclusions generally show larger elemental and isotopic compositional variation than their host lavas and the origin of these heterogeneities remains disputed. Here we present oxygen isotope data from melt inclusions hosted in olivine from two samples from the Mid-Atlantic ridge. Melt inclusions from different crystals within the same sample show more than 2.5‰ $\delta^{18}O$ variation within

23 each sample, which is nearly eight times the analytical error of 0.3‰ (2 standard deviations)

24 and five times the $\delta^{18}O$ range in unaltered MORB. Measured $\delta^{18}O$ in melt inclusions do not

25 correlate with common magmatic tracers, and $\delta^{18}O$ measured in the host olivines suggest a

26 maximum of 1‰ $\delta^{18}O$ source heterogeneity. Less than half of the melt inclusions from each

27 sample are in equilibrium with their host crystals; the remaining melt inclusions have either

28 lower or higher olivine-melt oxygen isotope partition coefficients compared to the theoretical

29 equilibrium values. Here we discuss several potential processes that could contribute to these

30 observations, but none satisfactorily explain the olivine-melt inclusion oxygen disequilibrium

31 that we observe in these samples. Nevertheless, it seems clear that the variability of $\delta^{18}O$ in

32 melt inclusion from two MORB samples do not record only common magmatic process(es),

33 but rather a localized grain scale process. Any $\delta^{18}O$ variation in melt inclusions should thus be

34 interpreted with caution.

35

36 **Keywords**

37 Olivine-hosted melt inclusions; MORB; Mid-Atlantic Ridge; oxygen isotopes; grain scale

38 processes; heterogeneity; SIMS

39

40 **Introduction**

41 Olivine-hosted melt inclusions are often used to study the origin and evolution of mantle-

42 derived magmas (for a review, see Kent, 2008; Schiano, 2003 and references therein). Melt

43 inclusions are physically isolated from their host magma, which undergoes different processes

44 during magmatic evolution after the entrapment of melt inclusions (for example, magma

45 mixing, assimilation, degassing). An important observation is that larger elemental and

46   isotopic compositional variations are generally observed in melt inclusions when compared to

47   whole-rock or glass compositions. A widespread interpretation is that variations measured in

48   melt inclusions reflect magmatic diversity that is not recorded in whole rock compositions

49   due to obscuration during later processes (e.g., Kent, 2008). In some cases, variations could

50   also be related to small-scale reactions in the melt in which the olivine is growing

51   (Danyushevsky et al., 2004).

52   In mid-oceanic ridge basalts (MORB), most melt inclusions have trace-element compositions

53   in the range of MORB lavas, but there are also some clear exceptions to this general

54   observation (see Schiano, 2003 for a review). These 'anomalous' trace-element compositions

55   have usually been interpreted to reflect near-fractional melting of a depleted mantle and/or

56   spinel lherzolite, or of hydrothermally altered peridotite (e.g., Gurenko and Chaussidon, 1995;

57   Nielsen et al., 2000; Sobolev and Shimizu, 1993). The anomalous trace-element compositions

58   are not found in MORB rocks, as MORBs represent aggregates of different melt fractions

59   (e.g., Jin et al., 1994; McKenzie, 1984; Sobolev and Shimizu, 1993). Melt reaction within the

60   crust, i.e. within a crystal mush, may also explain the larger compositional variations

61   observed in some MORB melt inclusions compared to lavas (e.g., Danyushevsky et al., 2004;

62   Kamenetsky and Gurenko, 2007).

63   Major and trace element variability in melt inclusions from MORB samples are also

64   sometimes observed within a single phenocryst (Shimizu, 1998), which indicates that melt

65   inclusions are not necessarily in equilibrium with their hosts. Such small-scale diversity could

66   be generated by trace element diffusion within the melt during melt inclusion formation by

67   host dissolution-reprecipitation, or by boundary layer entrapment during fast, diffusion-

68   controlled growth or melt transport (e.g., Baker, 2008; Cottrell et al., 2002; Faure and

69   Schiano, 2005; Manzini et al., 2017; Van Orman et al., 2002). Other processes, such as

70   diffusion of some elements (e.g., H, Fe) toward the host olivine or the host melt are

71   responsible, in some cases, for elemental variation in melt inclusions (e.g., Danyushevsky et

72   al., 2000a; Gaetani et al., 2012).

73   To date, no stable isotope data from melt inclusions within olivine from typical MORB

74   samples have been published. Although $\delta^{11}B$ and $\delta^{18}O$ were reported in some olivine-hosted

75   melt inclusions from Iceland, the petrogenetic history of these samples is fundamentally

76   different from typical MORB settings (Gurenko and Chaussidon, 1997, 2002; Hartley et al.,

77   2013). In this study, we focus on $\delta^{18}O$ values from melt inclusions within MORB samples, as

78   the systematics of this stable isotope system are well constrained. Based on a compilation of

79    $\delta^{18}O$ data in Neogene volcanic rocks, Harmond and Hoefs (1995) concluded that bulk MORB

80   rocks have $\delta^{18}O$ compositions of 5.7‰ ± 0.2‰. Because the variation reported is similar to

81   the typical analytical uncertainty reported in the literature for individual $\delta^{18}O$ measurements

82   of silicate rocks at that time, the authors concluded that MORB have a uniform $\delta^{18}O$

83   signature. More recently, fresh MORB glasses from the Mid-Atlantic Ridge, Indian Ocean

84   and east Pacific Ridge were analyzed by laser fluorination and show a narrow range of

85   oxygen isotope ratios from 5.37 ± 0.01 to 5.81 ± 0.04 ‰ (1σ), with an average of +5.50 ‰

86   (Eiler et al., 2000). In addition, $\delta^{18}O$ is thought to not fractionate during melting (e.g., Eiler,

87   2001). As such, if melt inclusions are representative of the MORB source, they should show

88   similar values within a relatively restricted range; however, as melt inclusions generally show

89   larger chemical variations than those recorded by the bulk rock, $\delta^{18}O$ in melt inclusions from

90   MORB samples might also display larger isotopic variabilities than MORB glasses.

91   Constraining the variability of oxygen isotopes in melt inclusions from MORB samples is

92   important, as $\delta^{18}O$ variations within these melt inclusions serve to assess the importance of

93   fluid interaction, magma mixing and/or assimilation of oceanic crust (Gurenko and

94   Chaussidon, 2002; Hartley et al., 2013). In this study we report $\delta^{18}O$ data from melt inclusions

95   within two different MORB samples from the northern Mid-Atlantic Ridge. We observe a

4

96   never before reported large range of $\delta^{18}O$ compositions within these melt inclusions, up to

97   2.5‰, and discuss the reported data in term of magmatic processes, olivine dissolution-

98   precipitation and diffusion.

99

Sample description and geological context

101   The studied olivine-hosted melt inclusions are from two dredged basalts from the North

102   Atlantic ridge. Sample ARP73-10-03 is a picrite from the FAMOUS zone (36°8372'N,

103   33°2482'W) that contains a little more than 20% olivine phenocrysts ($Fo_{87.2-91.3}$), rare

104   clinopyroxene, and plagioclase xenocrysts. The crystals are surrounded by a hyalocrystalline

105   groundmass composed of glass, plagioclase (An_{75-80}) and olivine microlites (Fo_{86}) (Laubier et

106   al., 2007). Laubier et al. (2007) suggest that the variable major and trace element

107   compositions of ARP73-10-03 melt inclusions reflect polybaric partial melting of a

108   homogeneous mantle, followed by mixing in various proportions at either different degrees of

109   melting or in different parts of the melting system.

110   CH77-DR6-203 is a dredged basalt from the 14° MAR triple junction (14.12°N, 45°W). This

111   fresh sample is highly enriched in volatiles, with CO_2 in vesicles and water in the glass,

112   (popping rock; Javoy and Pineau, 1991) and shows a compositional anomaly with enriched

113      $(Nb/Zr)_N$, $(Ta/Hf)_N$ and $(La/Sm)_N$ compared to adjacent segments which may result from

114   mantle heterogeneity (Bougault et al., 1988). The mantle heterogeneity hypothesis is also

115   supported by Sr and Nd isotopes in MORB rocks from different segments of the triple

116   junction (Dosso and Bougault, 1986). The melt inclusions studied here are hosted in 1-5 mm,

117   polyhedral olivines containing one or several melt inclusions. They are glassy, sub-spherical,

118   and have a radius of 40-350 μm. They contain no daughter minerals. Rare shrinkage bubbles

119   are present, but represent only a small fraction of the total volume.

120

Methods

121

122

Sample preparation

123

Polished olivines containing exposed melt inclusions were pressed into 1-inch indium mounts, along with the glass standards (BHVO-2G, BCR-2G and BIR-1G) and San Carlos olivine. Care was taken to mount them within 8 mm of the center of the mount. A separate mount was made for each sample. SEM images were acquired at the University of Lausanne using a Tescan Mira LMU field-emission scanning electron microscope operated at 20 kV and 0.2-0.4 nA probe current to ensure that the melt inclusions were totally glassy. Melt inclusions with cracks or crystals were discarded. Topography of each mount was measured using a Brucker GTA-K white light interferometer.

132

Electron microprobe

133

Major element compositions and X-ray distribution maps of melt inclusions and olivines were acquired using a JEOL 8200 Superprobe electron microprobe analyzer. Analytical conditions for the quantitative measurement of olivine were 15kV at 20nA and a 5 μm beam diameter. Counting times were 30 s for Si, Mg, Mn and Fe and 40 s for Al, Ca, Ni and Cr. Analytical conditions for analyses of melt inclusions were 15kV, 10 nA and a 10 μm beam diameter. Counting times were 30 s for all elements except for K (20 s) and Na (16 s). A glass standard (KL2-G) was used for SiO_2 and Al_2O_3. All other elements were calibrated on minerals. A grain of ML3B-G was used as an internal standard to check the calibration.

142

Secondary ion mass spectrometer

Oxygen isotope ratios, volatiles (H_2O, CO_2, Cl, F) and trace-element (Ti, V, Sr, Y, Nb, Ba, La, Ce, Nd, Sm, Eu, Yb) concentrations were determined using the CAMECA ims1280-HR at the SwissSIMS laboratory.

Oxygen isotopes

Analytical conditions were similar to those described by Seitz et al. (2017): Throughout $^{18}O/^{16}O$ measurements of melt inclusions and olivines, the sample was sputtered with a Cs^+ primary beam of 2 nA, which was raster over 15 μm. An electron gun was utilized in order to compensate for sample charging. Samples were pre-sputtered for 30 s, followed by 80 s of analysis (20 cycles of 4 s). Automatic centering of secondary ions on field and contrast apertures were performed before each analysis. Measurements of ^{16}O and ^{18}O were performed simultaneously via two Faraday cups, using 10^{10} and 10^{11} resistors, respectively. The intensity of ^{16}O was typically ~ 2.2×10^9 counts per second for glasses and ~1.7×10^9 counts per second for olivine. Internal error (2 standard error), reflecting the counting statistics of one analysis, was usually better than 0.3‰ for melt inclusions and olivines.

For melt inclusions, instrumental mass fractionation (IMF) was corrected using a set of 9 international glass standards with compositions ranging from basaltic to rhyolitic (NKT-1G, GOR132-2G, BIR-2G, BHVO-2G, ML3B-2G, BCR-2G, StHs6/80G, UoE-Lipari, ATHO-G; Hartley et al., 2012; Jochum et al., 2006). The matrix effect was corrected using a linear regression of IMF with SiO_2 (Figure DR1-A). Two to three standards (BHVO, BIR and BCR), with compositions closely bracketing the melt inclusion compositions, were added on each mount to monitor and correct for potential instrumental drift. For olivines, IMF was corrected using an in-house San Carlos olivine standard (Fo 90.1), as well as three in-house olivine reference materials (Fo 99.6, Fo 91.9 and Fo 37.5; Fig DR1-B).

167   At the outset of each session, we performed at least eight measurements of a running standard

168   (i.e., measured repeatedly during the session; BHVO for melt inclusions sessions and San

169   Carlos for olivine sessions), in order to determine standard reproducibility (noted hereafter in

170   2 standard deviation, 2SD). The 2 SDs were better than 0.3‰ for melt inclusions sessions,

171   and 0.4‰ for olivines sessions. To monitor the instrument stability, running standards were

172   measured every 8 to 12 unknowns and gave a reproducibility of 0.3‰ 2SD, similar to the

173   eight measurements at the outset of each session. Accuracy was checked using one of the two

174   to three standards inserted in each mounts and was similar to reproducibility (0.3‰ 2SD and

175   0.4‰ 2SD for melt inclusions and olivines, respectively).

176

177   *Trace elements*

178   Phosphorous concentrations within melt inclusions were measured using the same analytical

179   conditions described by Manzini et al. (2017): Trace-element compositions of melt inclusions

180   and olivine were analyzed using a 5-6 nA O$^-$ primary ion beam, resulting in an analysis spot

181   of about 20 μm. A mass resolution of 5000 was used. Samples were pre-sputtered for 90 s,

182   using a 25 μm raster. Trace elements were quantified by measuring the signal from the

183   following isotopes: ^{48}Ti, ^{51}V, ^{88}Sr, ^{89}Y, ^{93}Nb, ^{138}Ba, ^{139}La, ^{140}Ce, ^{142}Nd, ^{152}Sm, ^{153}Eu, ^{172}Yb.

184   These measurements were performed in mono-collection mode by peak switching throughout

185   one analytical run on an electron multiplier (EM) collector. ^{40}Ca was measured on a FC

186   collector in the same analytical run as the other trace elements and was used as reference

187   element. Using ^{40}Ca instead of ^{30}Si (or ^{28}Si) during melt inclusion analyses allowed us to

188   check for possible contamination by olivine throughout the analyses. A waiting time was used

189   to obtain a steady state sputtering condition, and each analysis consisted of six cycles.

190   Waiting and counting time, typical standard reproducibility and typical internal error are

191   given in Table DR1. BHVO-2G was used as standard for melt inclusions, using the USGS

192   certified values for the trace elements.

193

194   *Volatile elements*

195   A Cs^+ primary ion beam with a current of 1.5 nA was used to measure volatile elements

196   (H_2O, CO_2, Cl, F, S); throughout these analyses an electron gun was used to compensate the

197   charges and to avoid charging of the sample surface. The secondary beam was accelerated at

198   10 kV, and the sample was pre-sputtered applying a 15 μm raster for 210 s. Elements were

199   measured in mono-collection mode, with a 10 μm raster during 12 cycles. Total analysis time,

200   including pre-sputtering, was approximately 14 minutes. The field aperture was set to 3000

201   μm, entrance slit to 60 μm and exit slit to 240 μm. This configuration allowed a mass

202   resolution of 5000, sufficient to fully discriminate the interferences. BHVO-2G, BCR-2G,

203   BIR-1G, ALL, NS and ALV (Helo et al., 2011) were used as standards. BHVO-2G was then

204   used as a running standard to check instrument stability. Background was determined by

205   analysis of a synthetic anhydrous olivine. Additional information is given in Table DR1.

206

207   **Results**

208   A total of 34 melt inclusions within 30 olivines were measured from sample CH77-DR6-203,

209   as were 17 melt inclusions within 13 olivines from sample ARP73-10-03. The results of these

210   analyses are summarized in Table DR2. Oxygen isotope ratios in olivines are reported in

211   Table DR3.

212   Analyzed olivines are characterized by a high forsterite content (Fo = Mg/Fe+Mg) ranging

213   from 88.8 to 91.4 for ARP73-10-03 and from 84.0 to 90.9 for CH77-DR6-203. Major-element

214   compositions of melt inclusions were corrected for the effect of post-entrapment

215   crystallization (PEC) of olivine at the wall of melt inclusion, using the Petrolog software

216   package (Danyushevsky and Plechov, 2011). Parameters used for Petrolog calculations are

217   summarized in the footnote of Table DR2. Our calculated PEC indicates that between 5.9 and

218   18.1% of olivine crystallized after melt inclusion trapping. Major elements are less variable

219   after PEC correction (e.g., SiO_2 variation of 2.8 wt. % before and 1.6 wt. % after correction;

220   Table DR2), and all major-element compositions mentioned hereafter are corrected for PEC.

221   Melt inclusions from ARP73-10-03 have a narrow range of major-element compositions, with

222   SiO_2 ranging from 50.0-50.4 wt. %, MgO from 11.2-12.8 wt. % and K_2O from 0.10-0.15 wt.

223   %. CH77-DR6-203 shows a slightly larger compositional range in major elements, with SiO_2

224   content from 49.2-50.8 wt. %, MgO from 7.8-10.0 wt. %, and K_2O from 0.20-0.55 wt %

225   (Figure 1A). Major-, volatile- (Cl, F, S) and trace-element concentrations measured in

226   ARP73-10-03 fall within the same range as those reported by Laubier et al. (2012) for melt

227   inclusions within the same sample and are consistent with glass N-MORB compositions

228   (Jambon et al., 1995; Naumov et al., 2014; Wallace and Carmichael, 1992). Water and CO_2

229   concentrations are also in the typical range of MORB glass values (Danyushevsky et al.,

230   2000b; Magenheim et al., 1995; Wallace and Carmichael, 1992). The melt inclusions from

231   CH77-DR6-203 are enriched in volatiles (to a lower extent for CO_2) when compared with

232   MORB glass values, and have trace-element compositions similar to typical E-MORB glasses

233   (e.g., Figure 1B modified from Gale et al., 2013).
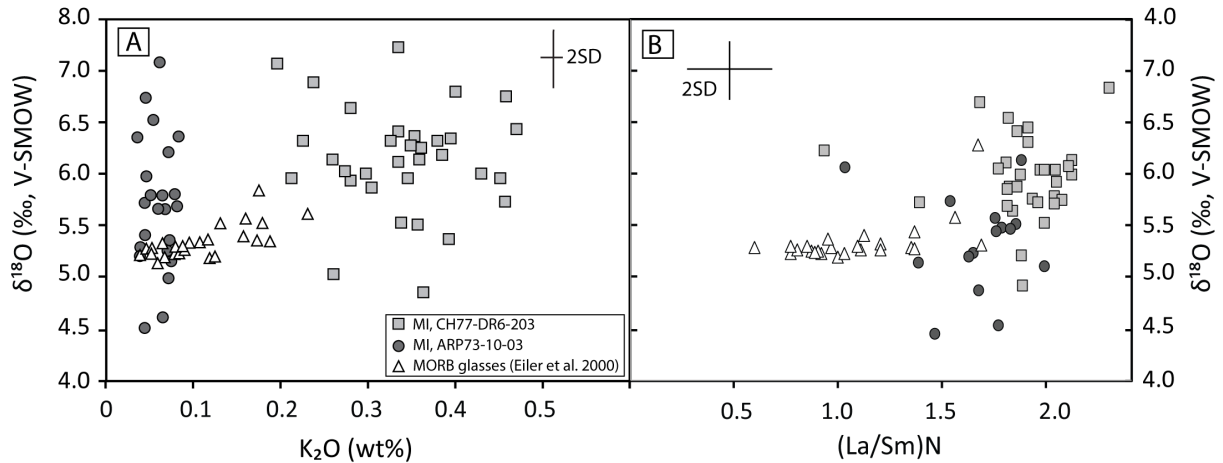
Figure 1: Oxygen isotope values for MI plotted against the K_2O concentration (A) and the La/Sm chondrite-normalized ratio (McDonough and Sun, 1995) (B). Line separating D-, N- and E-MORB are from Gale et al., 2013a. Fresh MORB glasses studied represented by white triangles in the figure, are plotted for comparison (Eiler et al., 2000).

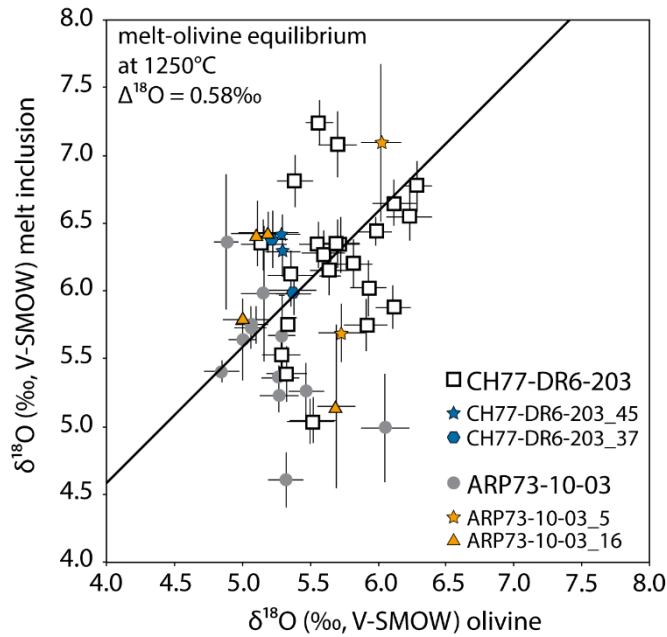Oxygen isotopes from melt inclusions show > 2.3‰ variation within each sample ($\delta^{18}O$ = +5.0 ± 0.17 to+7.2 ± 0.16‰, with an average of +6.2‰ for CH77-DR6-203; and $\delta^{18}O$ = +4.5 ± 0.3 to +7.1 ± 0.6‰, average +5.7‰ for ARP73-10-03). These variations are about eight times larger than the analytical uncertainty (0.3‰, 2SD) and about five times larger than the variations observed for bulk $\delta^{18}O$ of unaltered MORB glasses (<0.5‰; Figure 2). Before IMF correction, data show similar $\delta^{18}O$ variations (2.2‰). This is explained by the relatively narrow range of SiO_2 of the melt inclusions within a sample, which indicates that the applied IMFs are relatively similar (± 0.13‰) for all melt inclusions from the same sample. ARP73-10-03 is the closest to MORB glass composition in term of major, trace elements and oxygen isotopes. Nevertheless, 8 melt inclusions out of 21 have 'anomalous' $\delta^{18}O$ composition (i.e., statistically – 2 SD – outside the range of MORB glass bulk values). Within a single olivine, $\delta^{18}O$ from different melt inclusions are statistically different in the ARP73-10-03 sample (3 pairs, variation up to 2.2‰), whereas in the CH77-DR6-203 sample, melt inclusions hosted in

253   a single olivine have values within analytical uncertainty $\delta^{18}O$ (3 pairs, variation less than

254   0.4‰; Figure 3). In both samples, olivines show smaller variability than their hosted melt

255   inclusions: the ARP73-10-03 olivine have $\delta^{18}O$ values of +4.9 to +5.7‰ and olivines from

256   CH77-DR6-203 have $\delta^{18}O$ ranging from +5.0 to +6.5‰ (Table DR3, Figure 2).
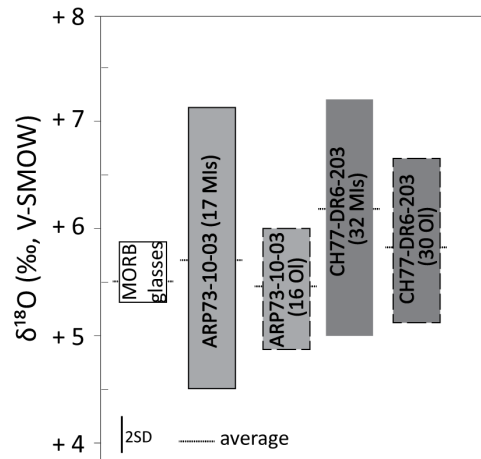
258   **Figure 2**: Comparison of oxygen isotope variations in MORB glasses from Mid-Atlantic Ridge,

259   Indian ocean and east-Pacific Ridge (n = 28) (Eiler et al., 2000) and melt inclusions (MIs) from the

260   two studied MORB samples (ARP73-10-03 and CH77-DR6-203). For a comparison, range of $\delta^{18}O$

261   composition measured in the olivines hosting the melt inclusions are also plotted (dashed line

262   contoured fields). Melt inclusions show larger variability compare to MORB glasses and to their host

263   olivines.

264

Figure 3: Oxygen isotope ratio of melt inclusions, compared to the $\delta^{18}O$ of their host olivine crystals. Melt-olivine equilibrium fractionation ($\Delta^{18}O$; black line) is from Matthews et al. (1998). Only 42 and 46% of melt inclusions from ARP_73-10-03 and CH77-203-DR6 are in equilibrium with their host, within analytical error.

Discussion

To date, no oxygen isotope data have been reported for olivine-hosted melt inclusions from MORB samples. Only two studies (Gurenko and Chaussidon, 2002; Hartley et al., 2013) reported $\delta^{18}O$ in olivine-hosted melt inclusions, and these data are from 7 samples taken from Iceland. These studies found $\delta^{18}O$ variation reaching a maximum of 1.2 ‰ (+4.0 to +5.2‰, sample 14161G, n = 3 melt inclusions; Gurenko and Chaussidon, 2002) and 0.95 ‰ (+3.05 to +4.0‰, sample N18, n = 9 melt inclusions; Hartley et al., 2013), respectively. These variations were interpreted to reflect either mixing of the ascending magma with melt lenses that had previously interacted with the low-$\delta^{18}O$ Icelandic crust (Hartley et al., 2013), or heterogeneity in the Icelandic mantle or mixing of two end-members (Gurenko and

280   Chaussidon, 2002). Melt inclusions from the two MORB samples measured in our study both

281   show more than 2.3‰ variation in $\delta^{18}O$, a larger variation than that reported for olivine-

282   hosted melt inclusions from Iceland. Hereafter, the $\delta^{18}O$ variability is discussed in term of

283   analytical versus magmatic processes.

284

285   *Analytical artefacts*

286   Oxygen isotope analyses via SIMS are very sensitive to the sample geometry, i.e. the

287   placement of the analyzed grains in the mount and the topography of the analyzed material

288   (e.g., Kita et al., 2009). All grains and reference material have been placed within 8 mm of the

289   center of the mount, in order to avoid X-Y effects due to deformation of the electrostatic field

290   close to the edge of the sample holder (Peres et al., 2013) (see methods section for more

291   details). Reproducibility of the measurements of a homogeneous reference material for

292   oxygen isotope is typically <0.3‰ (2 SD) when the surface relief is 1 μm, whereas it

293   increases up to 3‰ (2SD) when topography is on the order of 10-40 μm (Kita et al., 2009).

294   Our mounts show < 4 μm topography both between the indium and grains, and between

295   olivine and melt inclusions. Two different cases are presented in Figure 4: First, Figure 4-A

296   shows olivine CH77-DR6-203_37 hosting 2 melt inclusions with similar $\delta^{18}O$ (within the

297   0.3‰ 2SD calculated for a session, +6.37±0.21‰ and +5.97±0.16‰) and a topography of

298   1μm. Olivine ARP73-10-03_16, shown in Figure 4-B, has $\delta^{18}O$ in melt inclusions which vary

299   from +5.15 ± 0.21‰ to +6.42 ± 0.26‰. This olivine has a topographical variation of up to 4

300   μm, with a difference in topography of 1.5 μm between melt inclusions A, C and D

301   (maximum 1.3‰ difference in $\delta^{18}O$), and 2.5 μm between melt inclusions A and B (similar

302     $\delta^{18}O$). Melt inclusions are less than 1 μm lower compared to the olivine, which should not

303   affect the analyses: 17 analyses made following 2 profiles along perpendicular axes from wall

304   to wall in melt inclusion A, and 7 in melt inclusion B yield a reproducibility better than 0.3‰

305   (2SD) (Table DR2). Also, multiple measurements (n = 75) located at the edge or in the center

306   of the olivine grain ARP73-10-03_16, which shows the largest topographical variation, yield

307   data clustering within 0.45‰ (2SD; Table DR3), comparable to the reproducibility obtained

308   during the same session for San Carlos reference material that has negligible topography

309   (0.40‰, 2SD). Moreover, $\delta^{18}O$ from melt inclusions within ARP73-10-03_16 A and B were

310   measured twice, in two different sessions and similar values were obtained. As the mount was

311   placed in the sample holder with a different orientation, this confirms that measured $\delta^{18}O$

312   variation cannot be due to sample topography or orientation. Based on these observation, we

313   find it highly unlikely that topography of the grains is responsible for the large variation of

314     $\delta^{18}O$ in the melt inclusions analyzed in this study. As the calibration of the SIMS analyses

315   reported here were made using several reference materials covering the range of melt

316   inclusions major elements (Fig. DR2). Hence we conclude that the observed $\delta^{18}O$ variations

317   are real in melt inclusions and do not represent analytical artefacts.
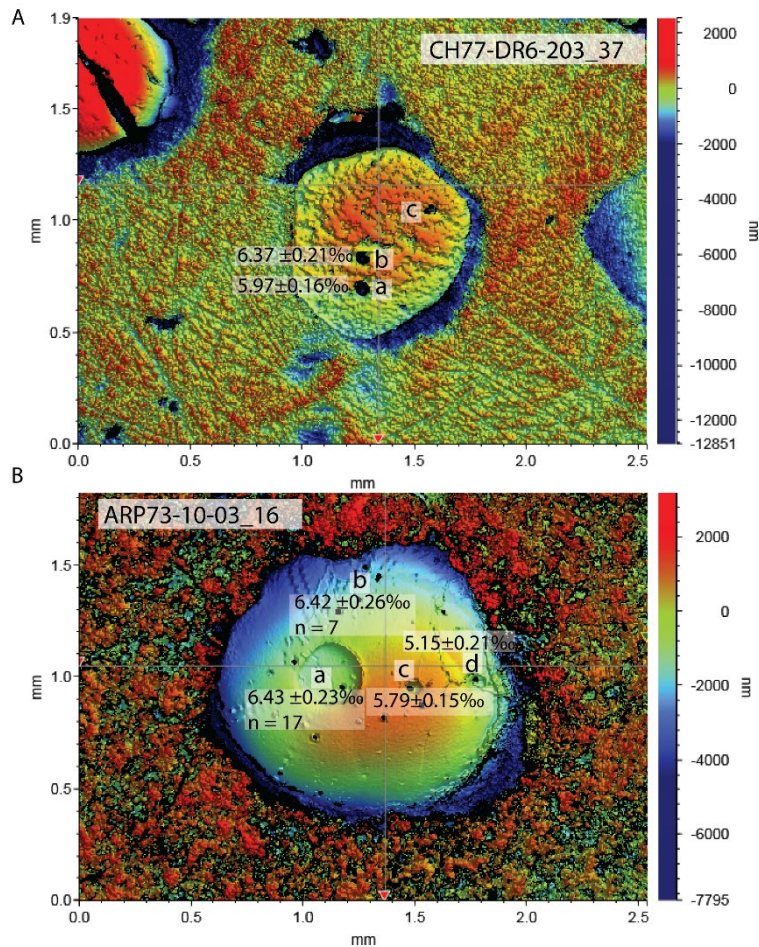
Figure 4: Example of profilometer images of the studied samples. A – ARP73-10-03_16 olivine; B – CH77-DR6-203_37 olivine. The number of points is specified when more than one analyses was obtained in the same inclusion, and the error (2SD) represents the reproducibility on the repeated measurements.

Effects of different magmatic processes

Partial melting causes large variations in the major- and trace- element concentrations of MORBs (e.g., Frey et al., 1993; Schilling et al., 1983; Zindler et al., 1979), but is not expected to largely fractionate oxygen isotopes. Indeed, Bindeman et al. (2012) estimate that extraction of 15% of the melt, assuming equilibrium is maintained throughout the melting, will change $\delta^{18}O$ by only 0.05‰. Even high degrees of partial melting (up to 42%) of a mantle source will

330   create less than 0.2 ‰ $\delta^{18}O$ variations (e.g. Eiler, 2001). Variation in the degree of partial

331   melting will thus not be resolvable by SIMS, given the typical precision of ~0.3‰ 2SD.

332   Hence, the lack of correlation between $\delta^{18}O$ and the abundance of incompatible elements such

333   as $[La/Sm]_N$ for example (Figure 1), which are sensitive to degree of melting, indicates that

334   variable extents of partial melting cannot explain the large $\delta^{18}O$ scatter measured in this study.

335   Interestingly, ARP73-10-03 has a composition similar to that of typical MORB glass (N-

336   MORB) in terms of $[La/Sm]_N$, K_2O and volatile contents, and average $\delta^{18}O$ composition (e.g.,

337   Eiler et al., 2000; Gale et al., 2013), whereas CH77-DR6-203 has higher $(La/Sm)_N$, volatiles,

338   K_2O contents, and $\delta^{18}O$ than that of N-MORB glass (Figure 1). Differences in $(La/Sm)_N$,

339   volatiles and K_2O contents between the two samples could reflect different degrees of

340   melting, but the different average $\delta^{18}O$ rather suggests melting of an enriched mantle source

341   for CH77-DR6-203. Despite the melting of different mantle sources for the two samples,

342   resulting in different $\delta^{18}O$ for their respective melt inclusions, a similar variation of $\delta^{18}O$

343   (~2.5‰) is observed in melt inclusions for both samples.

344   The lack of correlation between $\delta^{18}O$ of the melt inclusions and the forsterite content of their

345   host olivines do not support large fractionation of oxygen isotopes during magmatic evolution

346   of the studied samples (Figure 5). This observation is consistent with an experimental study

347   examining crystallization of a MORB melt dominated by olivine and plagioclase fractionation

348   (Tormey et al., 1987), which shows that the oxygen isotopic composition of the melt should

349   not vary by more than 0.1 ‰ for a MgO content between 3 to 8 wt% (Eiler, 2001). Recently,

350   Bucholz et al. (2017) modelled change in $\delta^{18}O$ in tholeiite during fractional crystallization and

351   also found minor change in $\delta^{18}O$ (up to 0.35‰ for composition comparable to ARP73-10-03

352   and CH77-203-DR3 melt inclusions).
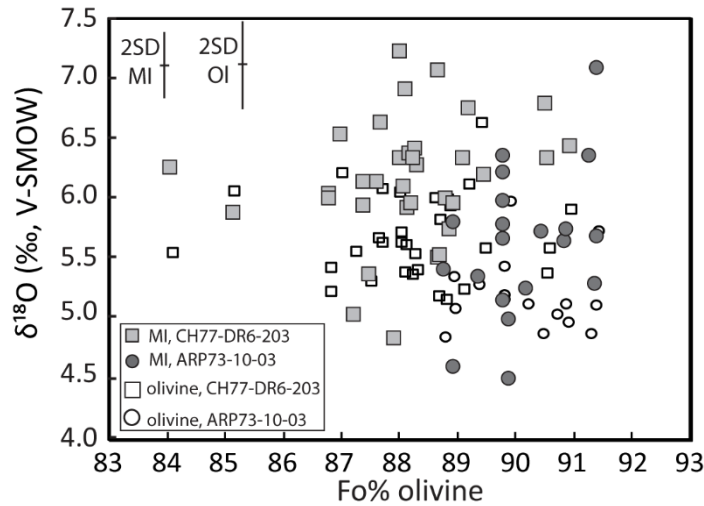
Figure 5: Plot of oxygen isotopes of olivine and of melt inclusions plotted against the Fo content of the host olivines. Full symbols are for melt inclusions, empty symbols represent olivines.

Considering the low volatile concentrations in MORB lavas, the effect of magma degassing on oxygen isotopes should be negligible. In fact, the total devolatilization of MORB magmas will change the $\delta^{18}O$ by less than 0.1 ‰ (Eiler, 2001). Similarly, oxygen fugacity changes in the magmatic system should not create any oxygen isotope ratio variations as the fractionation of oxygen isotopes in the melt is not controlled by fO_2 (Lester et al., 2013).

Assimilation of altered oceanic (AOC) crust with variable $\delta^{18}O$ (1-6‰ for lower AOC and 7-15‰ for upper AOC; e.g. Alt, 2003; Alt and Bach, 2006) may also affect the $\delta^{18}O$ variability observed in melts (e.g., Genske et al., 2013). The assimilation process can be modeled by simple mixing, because MORB melts and AOC have very similar oxygen concentrations. If we consider a typical mantle composition of $\delta^{18}O$=5.5 ‰ (Eiler, 2001; Mattey et al., 1994) and mix it with an altered upper oceanic crust with $\delta^{18}O$=15 ‰ (e.g., Alt, 2003), a minimum of 17% assimilation of upper AOC is required to explain the highest $\delta^{18}O$ measured in melt inclusions (7.1‰) from ARP73-10-03. This amount of upper AOC assimilation (>17%) would, for example, result in Ba content of >62 ppm, assuming an average Ba content of the

371 upper AOC of 300 ppm (e.g., Kelley et al., 2003) and 13.9 ppm for uncontaminated MORB

372 (Hofmann, 1988). As melt inclusions from ARP73-10-03 (N-MORB sample), have Ba

373 contents typical of N-MORB (around 20 ppm; maximum 34 ppm Ba), we find that

374 assimilation of upper crustal material is not likely to be responsible for the high $\delta^{18}O$ values

375 measured in these melt inclusions. Similarly, a minimum of 22% assimilation of the upper

376 AOC is required to obtain the lowest $\delta^{18}O$ (4.5‰) of the melt inclusions, assuming an

377 extreme lower AOC composition of $\delta^{18}O=1‰$ (as in hydrothermal amphibolite veins; e.g.,

378 Alt and Bach, 2006). Assimilation of serpentinites that have $\delta^{18}O$ values of 2.0 to 6.7‰, with

379 most of the values <5‰ (Barnes et al., 2014; Boschi et al., 2008) would require a larger

380 amount of assimilation compared to AOC, and could not account for the $\delta^{18}O$ up to 7.1 ‰ or

381 down to 4.5 ‰.

382 The absence of correlation between elements that are similarly incompatible in the dissolution

383 reactions of pyroxene, plagioclase and spinel (e.g., S and Ce; Danyushevsky et al., 2004)

384 suggests that local grain-scale dissolution-reaction mixing processes (Danyushevsky et al.,

385 2004) is an unlikely process to explain the $\delta^{18}O$ variations in melt inclusions. In fact, open

386 system local dissolution of minerals formed in equilibrium with a basaltic melt will not

387 change the $\delta^{18}O$ composition of the ascending basaltic melt.

388 The $\delta^{18}O$ variability of 1.1 and 1.4 ‰ in the olivine crystals ($\delta^{18}O_{(Ol)}$) from ARP73-10-03 and

389 CH77-DR6-203 (Table DR3), respectively, is an indicator that these olivine crystals record

390 crystallization in a heterogeneous environment, or record a heterogeneous crystallization

391 history. Considering the typical reproducibility of olivine measurements of 0.4‰, these

392 variations are not likely to reflect analytical artefacts and should therefore represent real

393 heterogeneities. In fact, individual crystals are homogeneous within measurement uncertainty

394 of ca. 0.4 ‰, while different crystals from the same sample are more variable. In terms of

395 major elements, each crystal is homogeneous (with the exception of P heterogeneities in some

396   olivines; Manzini et al., 2017), but all olivines have different Fo contents (Table DR3).

397   Within each sample, no clear trend is observed between Fo content and average $\delta^{18}O_{(Ol)}$ (Fig.

398   5). At a given Fo content, $\delta^{18}O_{(Ol)}$ varies up to 0.9‰. This observation suggests that these

399   olivine crystals from both samples grew in slightly heterogeneous environments (~0.9-1‰

400   variation).

401

Olivine-melt inclusion isotopic disequilibrium

403   Equilibrium fractionation between olivine and melt ($\Delta^{18}O_{ol-melt}$) at 1250°C is -0.6 ‰, based on

404   Matthews et al. (1998), which is equivalent to twice the uncertainty of the measured

405   compositions. As mentioned above, $\Delta^{18}O$ variability in the studied melt inclusions is larger

406   than the heterogeneity of their host olivines. Only 42 and 46% of melt inclusions from

407   ARP_73-10-03 and CH77-203-DR6 are in equilibrium with their host (Figure 3). The

408   remaining melt inclusions have either lower or higher $\Delta^{18}O_{ol-melt}$ compared to the theoretical

409   equilibrium value at 1250°C. While the proportion of melt inclusions in equilibrium with their

410   host olivine is similar for both samples, the proportion of melt inclusions with higher versus

411   lower $\Delta^{18}O_{ol-melt}$ is different for each sample. In detail, within an olivine containing several

412   exposed melt inclusions, $\Delta^{18}O_{ol-melt}$ can vary significantly. No correlation is observed between

413   olivine-melt isotopic disequilibrium and Fo content of the host olivine, which indicates that

414   disequilibrium conditions could have prevailed at any time during the samples' magmatic

415   history. An important observation is that melt inclusions in equilibrium with their host

416   olivines do not show significant $\delta^{18}O$ variation (5.7±0.3‰ for ARP73-10-03 and 6.3±0.5‰

417   for CH77-203-DR6). Assuming equilibrium between olivine and melt, variations in

418   temperature throughout crystal growth could affect $\Delta^{18}O_{ol-melt}$. However, the large variation of

419     $\Delta^{18}O_{ol-melt}$ would require a large and unrealistic temperature range, from 700°C for the lowest

420     $\Delta^{18}O_{ol-melt}$ to >2500 °C for the positive $\Delta^{18}O_{ol-melt}$.

421   We propose that the measured $\Delta^{18}O_{ol\text{-}melt}$ variations instead indicate disequilibrium. Lower or

422   higher $\Delta^{18}O_{ol\text{-}melt}$ compared to theoretical equilibrium require either a process able to shift the

423   equilibrium toward both higher and lower values, or a combination of different processes.

424   Oxygen diffusion along the moving interface between melt and crystal during crystal growth

425   or after melt inclusion entrapment is a process capable of generating isotopic disequilibrium

426   between melt inclusions and their host olivine. Rapid crystal growth can lead to a local

427   disequilibrium in the growth media, creating boundary layers in which elements with the

428   lowest diffusivity in the melt and/or lowest partition coefficients (e.g., S, Cl, P, Al) will

429   concentrate. It has been demonstrated that this process can create melt inclusion compositions

430   with different major elements (Faure and Schiano, 2005; Watson and Müller, 2009), volatiles

431   (S, Cl) and/or P content (Baker, 2008) compared to the bulk melt composition. Oxygen is also

432   a slow diffusing element in relatively dry melts, with ^{16}O diffusing faster than ^{18}O (e.g.,

433   Lesher, 2010); therefore, such a boundary layer should have a higher $\delta^{18}O$ composition than

434   the melt in which the crystal in growing. Melt inclusions from ARP-73-10-03 have major,

435   trace and volatile elements compositions similar to MORB, with no enrichment in Al, S, Cl or

436   Ca; however, some melt inclusions within this sample do have higher P contents due to

437   olivine dissolution near P-rich (fast growing) domains (Manzini et al., 2017). No significant

438   difference in $\delta^{18}O_{(Ol)}$ between P-rich and P-poor domains within each olivine are observed

439   (Figure DR2). Moreover, $\delta^{18}O_{(Ol)}$ compositions of the recrystallized olivine (P-depleted halo)

440   are similar to those of the primary olivine (Figure 6A). Figure 6B shows the $\delta^{18}O$ of melt

441   inclusions from both samples, as a function of their location (in primary olivine, or in

442   recrystallized domains), based on phosphorus maps of the host olivines. No systematic shift in

443    $\delta^{18}O$ as a function of the olivine domain in which the melt inclusion is trapped can be

444   resolved. Also, isotopic disequilibrium can be found in melt inclusions trapped in olivine with

445   or without P zoning (Table DR2), suggesting that the MI-Olivine $\delta^{18}O$ disequilibrium and

446 large $\delta^{18}O$ variations in melt inclusions are not related to initial rapid crystal growth creating

447 P-rich domains, nor to the dissolution of P-rich olivine domains.
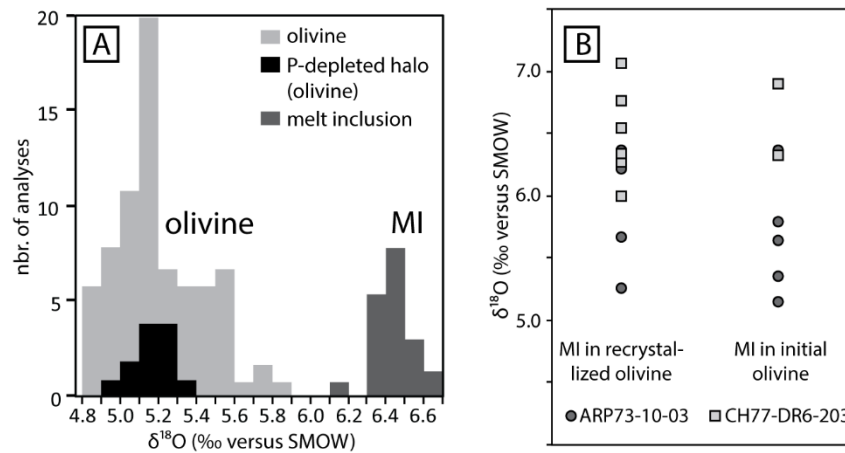
448

449 **Figure 6**: **A**: Comparison of $\delta^{18}O$ measured in the ARP73-10-03_16 olivine (P-enriched and P-normal

450 zones), in the re-precipitated part (P-depleted zone around melt inclusion) and in the 2 melt inclusions

451 situated in the P-zoned olivine part. No differences in oxygen isotope can be seen between the

452 different parts of the olivine. **B**: Comparison of $\delta^{18}O$ measured in melt inclusions located in

453 recrystallized olivine (i.e. close to a P-zoned region of the olivine) and in unzoned olivine parts,

454 probably in initial olivine, that did not suffer from dissolution and re-precipitation. No differences can

455 be observed between the two populations, but in general CH77-DR6-203 has higher $\delta^{18}O$ values than
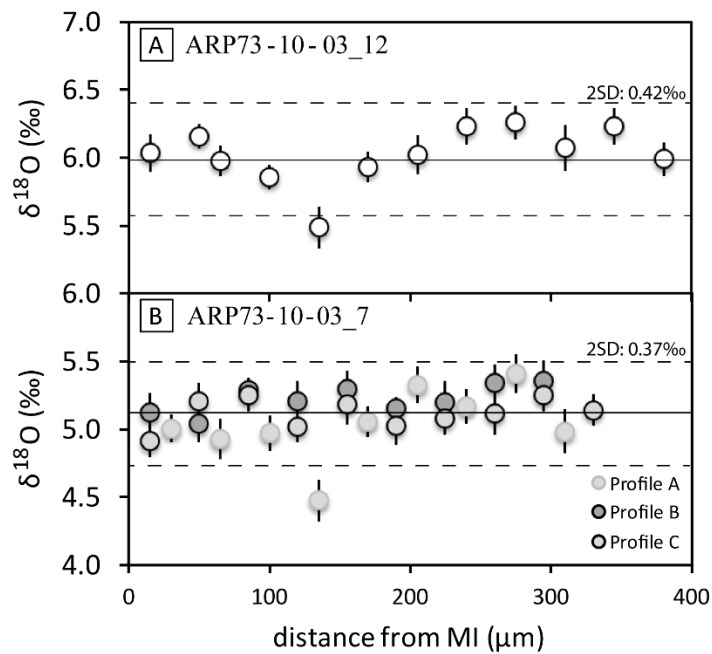
456 ARP73-10-03.

457

458 As argued above, olivine-hosted melt inclusions within the samples studied here suffered

459 from PEC of olivine. Manzini et al. (2017) have shown that this thin (< 1 μm) layer

460 crystallizes a few hours before eruption. This fast crystallization results in a strong P

461 enrichment of the late-crystallized olivine. Post-entrapment crystallization could thus generate

462 a thin boundary layer with a distinct (high) $\delta^{18}O_{(Ol)}$ composition and lower the initial $\delta^{18}O$ of

463 the melt inclusions. Given the small volume of the PEC (1 μm layer compared to melt

464 inclusion diameters of > 50 μm), it should not largely influence the melt inclusion

465 composition. This assumption is verified by the absence of a correlation between amount of

466 PEC or P with $\delta^{18}O$ of the melt inclusions or $\Delta^{18}O_{ol-melt}$.

467 Diffusion of O in and out of the melt inclusions could in theory produce higher or lower

468 $\Delta^{18}O_{ol-melt}$. Oxygen can diffuse as mono or multi-species. Indeed, O is present in CO_2 and

469 H_2O molecules. It is known that water can diffuse in or out of melt inclusions (e.g., Chen et

470 al., 2013; Gaetani et al., 2012; Portnyagin et al., 2008), but mostly in the form of H^+. Given

471 the low water content involved in MORB systems, this should not produce large $\delta^{18}O$

472 variations in melt inclusions (Zhang and Ni, 2010). It is possible that CO_2 could largely degas

473 in melt inclusion shrinkage bubbles (e.g., Moore et al., 2015); migration of CO_2 in the bubble

474 may fractionate $\delta^{18}O$, but as ^{16}O is diffusing faster this could only generate higher $\delta^{18}O$. Melt

475 inclusions with the lowest $\Delta^{18}O_{ol-melt}$ do not necessarily contain shrinkage bubbles, which

476 indicates that fractionation of O isotopes is not related to shrinkage bubble formation.

477 Diffusion of O after melt inclusion entrapment would imply that melt inclusions were initially

478 not in equilibrium with their host at the time of entrapment and thus cannot explain the origin

479 of the large variation of $\delta^{18}O$ in the studied melt inclusions. If O isotopic diffusion occurred

480 after melt inclusion entrapment, it should be limited based on the following observations:

481 First, based on P profiles made from melt inclusions in olivines, melt inclusions were trapped

482 for a few hours to a few days before quenching (Manzini et al., 2017). Using the diffusion

483 data of Dohmen et al. (2002) (this dataset yields a diffusion coefficient of $\sim9.3\times10^{12}$ in olivine

484 at 1250°C), this amount of time would result in a small amount of O diffusing from melt

485 inclusion to olivine over a profile no longer than 10 microns, which is not resolvable using the

486 techniques employed in this study. This is confirmed by $\delta^{18}O$ profiles obtained from three

487 different olivines, in which melt inclusions are either in disequilibrium (Figures 7A and DR2)

488 or equilibrium (Figure 7B), starting at $\sim$15-30μm from the inclusion wall, do not show any

489 significant increase or decrease of $\delta^{18}O$ values toward the MI. Second, $\delta^{18}O$ profiles measured

490 within a single melt inclusion, from olivine wall to MI center, give similar values (Figure 8).

491 Lastly, there is no correlation between the melt inclusion size and the $\delta^{18}O$ value of the melt

492 inclusion.

493

494 **Figure 7**: Oxygen isotopes profiles in olivines, starting from melt inclusion. A: oxygen isotopes

495 profile in olivine ARP73-10-03_12, for which melt inclusion "a" is not in equilibrium. Profile starts

496 from the melt inclusion. B: different $\delta^{18}O$ profiles done around the melt inclusion (in equilibrium)

497 entrapped in olivine ARP-10-03_7. The 3 profiles start from 3 different locations around the melt

498 inclusion and all are made in different directions. No clear diffusion profile from the melt inclusion

499 toward the olivine can be observed. Black lines represent the average composition of olivine and

500 dashed lines the 2 SD variations of the data along the profiles.

501
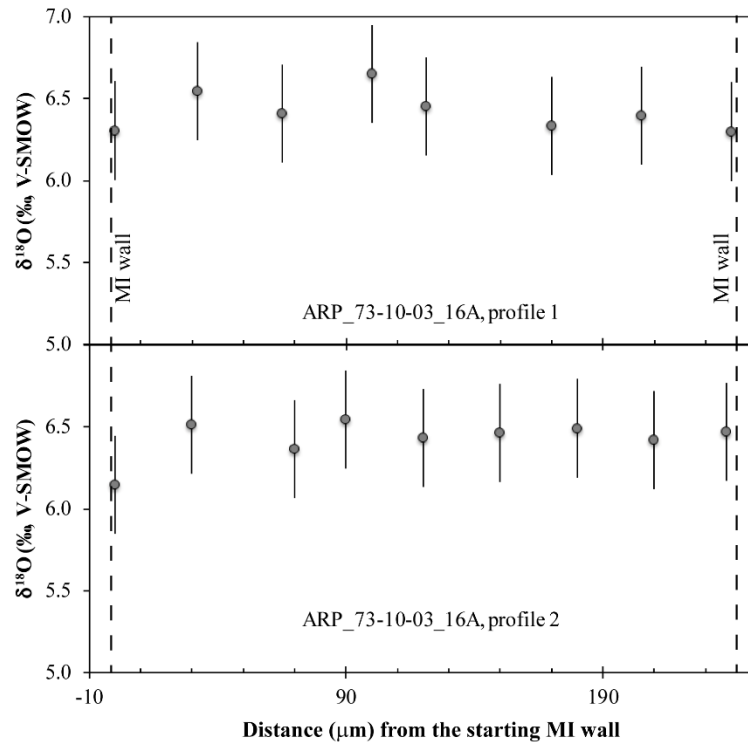
Figure 8: Oxygen isotopes profiles in melt inclusion APR-73-10-03_16A, from wall to wall. Two profiles were performed in this melt inclusion, perpendicular to one other.

In theory, oxygen diffusion could occur in response to a thermal gradient (Soret diffusion). Indeed, Kyser (1998) and Bindeman et al. (2013) reported significant isotopic fractionation of oxygen isotopes (up to 5.0‰) in anhydrous basaltic melt due to thermal diffusion, with migration of [18]O towards the colder regions. However, such a process has never convincingly been demonstrated in natural samples. Kyser (1998) pointed out that, even if thermally induced diffusion can lead to large $\delta^{18}O$ fractionation, the rapid decay of thermal gradient (< 10 days for 100° gradient at 1 cm from contact) makes it an unlikely process to happen in natural samples. Given the short timescale associated with the olivine residence time and melt inclusion formation in our samples (Manzini et al., 2017), a locally large thermal gradient (> 250°C) between migrating magma and conduit walls might be sustained before melt inclusion trapping. Assuming such a scenario, melt inclusions with $\delta^{18}O$ lower might form in olivine

517   located in the center of a conduit, whereas melt inclusions with higher $\delta^{18}O$ would form close

518   to the walls of the conduit; however, olivine crystallizing around the melt inclusions should

519   also have variable $\delta^{18}O$, which is not observed. This observation indicates that O diffusion in

520   response to a thermal gradient is not responsible for the $\delta^{18}O$ variation in melt inclusions.

521

Concluding remarks

523   The large variations (up to 2.5‰) observed in oxygen isotope ratios within melt inclusions

524   from 2 different Atlantic MORB samples (N-MORB and E-MORB) are not correlated with

525   major, trace or volatile elements. Oxygen isotope compositions of host olivines suggest a

526   small (<1‰) source heterogeneity for each sample. Less than half of the melt inclusions from

527   each sample are in isotopic equilibrium with their host olivines. The remaining melt

528   inclusions have either lower or higher isotopic fractionation compare to theoretical

529   equilibrium values. Boundary layer entrapment will only shift $\delta^{18}O$ toward higher values, and

530   the present dataset does not support this hypothesis. Fractionation diffusion of O during CO_2

531   migration into the shrinkage bubble will shift $\delta^{18}O$ toward lower values, but no evidence of

532   this process has been found. Another process capable of generating $\delta^{18}O$ fractionation both

533   higher and lower than equilibrium values is O diffusion in due to the presence of a thermal

534   gradient before melt inclusion entrapment (i.e. Soret diffusion). Although this process could

535   explain the large $\delta^{18}O$ variation measured, it would imply that a large, unrealistic, thermal

536   gradient (> 250°C) is sustained during the formation of melt inclusions. In addition, the

537   olivine directly surrounding the melt inclusion should also have a different $\delta^{18}O$ in this

538   scenario, which we do not observe.

539   Despite the marked disequilibrium in a majority of melt inclusions, our data do not show any

540   significant O diffusion in or out the melt inclusions. This is due to the short residence time at

high temperature after melt inclusion entrapment and the relatively large spatial resolution of the SIMS (10-15 microns). The exact process responsible for the melt inclusion-host $\delta^{18}O$ disequilibrium is thus not yet fully understood. Nonetheless, we argue that this dataset clearly shows that melt inclusions do not necessarily record the $\delta^{18}O$ composition of the magma in which their host grew. Caution should thus be taken before interpreting $\delta^{18}O$ variation as source process, especially when not related to any other tracer of common magmatic processes.

Acknowledgements

559

References

561 Alt, J.C., 2003. Stable isotopic composition of upper oceanic crust formed at a fast spreading ridge,

562   ODP Site 801. Geochemistry, Geophys. Geosystems 4, 1–11.

563   https://doi.org/10.1029/2002GC000400

564 Alt, J.C., Bach, W., 2006. Oxygen isotope composition of a section of lower oceanic crust, ODP Hole

565   735B. Geochemistry, Geophys. Geosystems 7. https://doi.org/10.1029/2006GC001385

566 Baker, D.R., 2008. The fidelity of melt inclusions as records of melt composition. Contrib. to Mineral.

567   Petrol. 156, 377–395. https://doi.org/10.1007/s00410-008-0291-3

568 Barnes, J.D., Beltrando, M., Lee, C.T.A., Cisneros, M., Loewy, S., Chin, E., 2014. Geochemistry of

569   Alpine serpentinites from rifting to subduction: A view across paleogeographic domains and

570   metamorphic grade. Chem. Geol. 389, 29–47. https://doi.org/10.1016/j.chemgeo.2014.09.012

571 Bindeman, I.N., Kamenetsky, V.S., Palandri, J., Vennemann, T., 2012. Hydrogen and oxygen isotope

572   behaviors during variable degrees of upper mantle melting: Example from the basaltic glasses

573   from Macquarie Island. Chem. Geol. 310–311, 126–136.

574   https://doi.org/10.1016/j.chemgeo.2012.03.031

575 Bindeman, I.N., Lundstrom, C.C., Bopp, C., Huang, F., 2013. Stable isotope fractionation by thermal

576   diffusion through partially molten wet and dry silicate rocks. Earth Planet. Sci. Lett. 365, 51–62.

577   https://doi.org/10.1016/j.epsl.2012.12.037

578 Boschi, C., Dini, A., Früh-Green, G.L., Kelley, D.S., 2008. Isotopic and element exchange during

579   serpentinization and metasomatism at the Atlantis Massif (MAR 30°N): Insights from B and Sr

580   isotope data. Geochim. Cosmochim. Acta 72, 1801–1823.

581   https://doi.org/10.1016/j.gca.2008.01.013

582 Bougault, H., Dmitriev, L., Schilling, J.G., Sobolev, A., Joron, J.L., Needham, H.D., 1988. Mantle

583   heterogeneity from trace elements: MAR triple junction near 14°N. Earth Planet. Sci. Lett. 88,

584   27–36. https://doi.org/10.1016/0012-821X(88)90043-X

585   Bucholz, C.E., Jagoutz, O., VanTongeren, J.A., Setera, J., Wang, Z., 2017. Oxygen isotope trajectories

586   of crystallizing melts: Insights from modeling and the plutonic record. Geochim. Cosmochim.

587   Acta 207, 154–184. https://doi.org/10.1016/j.gca.2017.03.027

588   Chen, Y., Provost, A., Schiano, P., Cluzel, N., 2013. Magma ascent rate and initial water

589   concentration inferred from diffusive water loss from olivine-hosted melt inclusions. Contrib. to

590   Mineral. Petrol. 165, 525–541. https://doi.org/10.1007/s00410-012-0821-x

591   Cottrell, E., Spiegelman, M., Langmuir, C.H., 2002. Consequences of diffusive reequilibration for the

592   interpretation of melt inclusions. New York 3.

593   Danyushevsky, L. V., Della-Pasqua, F.N., Sokolov, S., 2000a. Re-equilibration of melt inclusions

594   trapped by magnesian olivine phenocrysts from subduction-related magmas: Petrological

595   implications. Contrib. to Mineral. Petrol. 138, 68–83. https://doi.org/10.1007/PL00007664

596   Danyushevsky, L. V., Eggins, S.M., Falloon, T.J., Christie, D.M., 2000b. H_2O abundance in depleted

597   to moderately enriched mid-ocean ridge magmas; Part I: Incompatible behaviour, implications

598   for mantle storage, and origin of regional variations. J. Petrol. 41, 1329–1364.

599   https://doi.org/10.1093/petrology/41.8.1329

600   Danyushevsky, L. V., Leslie, R.A.J., Crawford, A.J., Durance, P., 2004. Melt inclusions in primitive

601   olivine phenocrysts: The role of localized reaction processes in the origin of anomalous

602   compositions. J. Petrol. https://doi.org/10.1093/petrology/egh080

603   Danyushevsky, L. V., Plechov, P., 2011. Petrolog3: Integrated software for modeling crystallization

604   processes. Geochemistry, Geophys. Geosystems 12. https://doi.org/10.1029/2011GC003516

605   Dohmen, R., Chakraborty, S., Becker, H.-W., 2002. Si and O diffusion in olivine and implications for

606   characterizing plastic flow in the mantle. Geophys. Res. Lett. 29, 2030.

607   https://doi.org/10.1029/2002GL015480

608   Dosso, L., Bougault, H., 1986. A hot spot at 14 N on the Mid-Atlantic Ridge: Isotopic (Sr, Nd) and

609   trace element data. Eos Trans. AGU 67, 410.

610   Eiler, J.M., 2001. Oxygen Isotope Variations of Basaltic Lavas and Upper Mantle Rocks. Rev.

611   Mineral. Geochemistry 43, 319–364. https://doi.org/10.2138/gsrmg.43.1.319

612   Eiler, J.M., Schiano, P., Kitchen, N., Stolper, E.M., 2000. Oxygen-isotope evidence for recycled crust

613   in the sources of mid-ocean-ridge basalts. Nature 403, 530–534.

614   Faure, F., Schiano, P., 2005. Experimental investigation of equilibration conditions during forsterite

615   growth and melt inclusion formation. Earth Planet. Sci. Lett. 236, 882–898.

616   https://doi.org/10.1016/j.epsl.2005.04.050

617   Frey, F.A., Walker, N., Stakes, D., Hart, S.R., Nielsen, R., 1993. Geochemical characteristics of

618   basaltic glasses from theamar andfamous axial valleys, Mid-Atlantic Ridge (36°–37°N):

619   Petrogenetic implications. Earth Planet. Sci. Lett. 115, 117–136. https://doi.org/10.1016/0012-

620   821X(93)90217-W

621   Gaetani, G. a., O'Leary, J. a., Shimizu, N., Bucholz, C.E., Newville, M., 2012. Rapid reequilibration

622   of H_2O and oxygen fugacity in olivine-hosted melt inclusions. Geology 40, 915–918.

623   https://doi.org/10.1130/G32992.1

624   Gale, A., Dalton, C.A., Langmuir, C.H., Su, Y., Schilling, J.-G., Dalton, C.A., Langmuir, C.H., Su, Y.,

625   Schilling, J., 2013. The mean composition of ocean ridge basalts. Geochem. Geophys. Geosyst

626   14, 489–518. https://doi.org/10.1029/2012GC004334

627   Garcia, M.O., Ito, E.M.I., Eiler, J.M., Pietruszka, A.J., 1998. Crustal Contamination of Kilauea

628   Volcano Magmas Revealed by Oxygen Isotope Analyses of Glass and Olivine from Puu Oo

629   Eruption Lavas 39, 803–817.

630   Genske, F.S., Beier, C., Haase, K.M., Turner, S.P., Krumm, S., Brandl, P.A., 2013. Oxygen isotopes

631   in the Azores islands: Crustal assimilation recorded in olivine. Geology 41, 491–494.

632   https://doi.org/10.1130/G33911.1

633   Gurenko, A.A., Bindeman, I.N., Chaussidon, M., 2011. Oxygen isotope heterogeneity of the mantle

634   beneath the Canary Islands: insights from olivine phenocrysts. Contrib. to Mineral. Petrol. 162,

635   349–363. https://doi.org/10.1007/s00410-010-0600-5

636   Gurenko, A.A., Chaussidon, M., 2002. Oxygen isotope variations in primitive tholeiites of Iceland :

637   evidence from a SIMS study of glass inclusions , olivine phenocrysts and pillow rim glasses.

638   Earth Planet. Sci. Lett. 205, 63–79.

639   Gurenko, A.A., Chaussidon, M., 1997. Boron concentrations and isotopic composition of the Icelandic

640   mantle: evidence from glass inclusions in olivine. Chem. Geol. 135, 21–34.

641   Gurenko, A.A., Chaussidon, M., 1995. Enriched and depleted primitive melts included in olivine from

642   Icelandic tholeiites: origin by continuous melting of a single mantle column. Geochim.

643   Cosmochim. Acta 59, 2905–2917. https://doi.org/10.1016/0016-7037(95)00184-0

644   Harmon, R.S., Hoefs, J., 1995. Oxygen isotope heterogeneity of the mantle deduced from global 18O

645   systematics of basalts from different geotectonic settings. Contrib. to Mineral. Petrol. 95–114.

646   Hartley, M.E., Thordarson, T., Fitton, J.G., 2013a. Oxygen isotopes in melt inclusions and glasses

647   from the Askja volcanic system, North Iceland. Geochim. Cosmochim. Acta 123, 55–73.

648   https://doi.org/10.1016/j.gca.2013.09.008

649   Hartley, M.E., Thordarson, T., Fitton, J.G., 2013b. Oxygen isotopes in melt inclusions and glasses

650   from the Askja volcanic system, North Iceland. Geochim. Cosmochim. Acta 123, 55–73.

651   https://doi.org/10.1016/j.gca.2013.09.008

652   Hartley, M.E., Thordarson, T., Taylor, C., Fitton, J.G., EIMF, 2012. Evaluation of the effects of

653   composition on instrumental mass fractionation during SIMS oxygen isotope analyses of glasses.

654   Chem. Geol. 334, 312–323. https://doi.org/10.1016/j.chemgeo.2012.10.027

655   Helo, C., Longpré, M.A., Shimizu, N., Clague, D.A., Stix, J., 2011. Explosive eruptions at mid-ocean

656   ridges driven by CO_2-rich magmas. Nat. Geosci. 4, 260–263. https://doi.org/10.1038/ngeo1104

657   Hofmann, A.W., 1988. Chemical differentiation of the Earth : the relationship between mantle ,

658   continental crust , and oceanic crust 90, 297–314.

659   Jambon, A., Déruelle, B., Dreibus, G., Pineau, F., 1995. Chlorine and bromine abundance in MORB:

660   the contrasting behaviour of the Mid-Atlantic Ridge and East Pacific Rise and implications for

661   chlorine geodynamic cycle. Chem. Geol. 126, 101–117. https://doi.org/10.1016/0009-

662   2541(95)00112-4

663   Javoy, M., Pineau, F., 1991. The volatiles record of a "popping" rock from the Mid-Atlantic Ridge at

664   14°N: chemical and isotopic composition of gas trapped in the vesicles. Earth Planet. Sci. Lett.

665   107, 598–611. https://doi.org/10.1016/0012-821X(91)90104-P

666   Jin, Z.-M., Green, H.W., Zhou, Y., 1994. Melt topology in partially molten mantle peridotite during

667   ductile deformation. Nature 372, 164.

668   Jochum, K.P., Stoll, B., Herwig, K., Willbold, M., Hofmann, A.W., Amini, M., Aarburg, S.,

669   Abouchami, W., Hellebrand, E., Mocek, B., Raczek, I., Stracke, A., Alard, O., Bouman, C.,

670   Becker, S., Dücking, M., Brätz, H., Klemd, R., de Bruin, D., Canil, D., Cornell, D., de Hoog, C.-

671   J., Dalpé, C., Danyushevsky, L., Eisenhauer, A., Gao, Y., Snow, J.E., Groschopf, N., Günther,

672   D., Latkoczy, C., Guillong, M., Hauri, E.H., Höfer, H.E., Lahaye, Y., Horz, K., Jacob, D.E.,

673   Kasemann, S.A., Kent, A.J.R., Ludwig, T., Zack, T., Mason, P.R.D., Meixner, A., Rosner, M.,

674   Misawa, K., Nash, B.P., Pfänder, J., Premo, W.R., Sun, W.D., Tiepolo, M., Vannucci, R.,

675   Vennemann, T., Wayne, D., Woodhead, J.D., 2006. MPI-DING reference glasses for in situ

676   microanalysis: New reference values for element concentrations and isotope ratios.

677   Geochemistry, Geophys. Geosystems 7, n/a-n/a. https://doi.org/10.1029/2005GC001060

678   Kamenetsky, V.S., Gurenko, A.A., 2007. Cryptic crustal contamination of MORB primitive melts

679   recorded in olivine-hosted glass and mineral inclusions. Contrib. to Mineral. Petrol. 153, 465–

680   481. https://doi.org/10.1007/s00410-006-0160-x

681   Kelley, K. a., Plank, T., Ludden, J., Staudigel, H., 2003. Composition of altered oceanic crust at ODP

682   Sites 801 and 1149. Geochemistry, Geophys. Geosystems 4, n/a-n/a.

683   https://doi.org/10.1029/2002GC000435

684   Kempton, P.D., Hawkesworth, C.J., Fowler, M., 1991. Geochemistry and isotopic composition of

685   gabbros from layer 3 of the Indian Ocean crust, Hole 735B. Proc., Sci. results, ODP, Leg 118,

686   Fract. Zo. Drill. Southwest Indian Ridge 127–143.

687   https://doi.org/10.2973/odp.proc.sr.118.118.1991

688   Kent, A.J.R., 2008. Melt Inclusions in Basaltic and Related Volcanic Rocks. Rev. Mineral.

689   Geochemistry 69, 273–331. https://doi.org/10.2138/rmg.2008.69.8

690   Kita, N.T., Ushikubo, T., Fu, B., Valley, J.W., 2009. High precision SIMS oxygen isotope analysis

691   and the effect of sample topography. Chem. Geol. 264, 43–57.

692   https://doi.org/10.1016/j.chemgeo.2009.02.012

693   Kyser, T.K., Lesher, C.E., Walker, D., 1998. The effects of liquid immiscibility and thermal diffusion

694   on oxygen isotopes in silicate liquids. Contrib. to Mineral. Petrol. 133, 373–381.

695   https://doi.org/10.1007/s004100050459

696   Laubier, M., Gale, A., Langmuir, C.H., 2012. Melting and crustal processes at the FAMOUS segment

697   (mid-atlantic ridge): New insights from olivine-hosted melt inclusions from multiple samples. J.

698   Petrol. 53, 665–698. https://doi.org/10.1093/petrology/egr075

699   Laubier, M., Schiano, P., Doucelance, R., Ottolini, L., Laporte, D., 2007. Olivine-hosted melt

700   inclusions and melting processes beneath the FAMOUS zone (Mid-Atlantic Ridge). Chem. Geol.

701   240, 129–150. https://doi.org/10.1016/j.chemgeo.2007.02.002

702   Lecuyer, C., Reynard, B., 1996. High-temperature alteration of oceanic gabbros by seawater (Hess

703   Deep, Ocean Drilling Program Leg 147): Evidence from oxygen isotopes and elemental fluxes. J.

704   Geophys. Res. 101, 15883–15897.

705   Lesher, C.E., 2010. Self-diffusion in Silicate Melts: Theory, Observations and Applications to

706   Magmatic Systems. Rev. Mineral. Geochemistry 72, 269–309.

707   https://doi.org/10.2138/rmg.2010.72.7

708   Lester, G.W., Kyser, T.K., Clark, A.H., 2013. Oxygen isotope partitioning between immiscible silicate

709   melts with H_2O, P and S. Geochim. Cosmochim. Acta 109, 306–311.

710   https://doi.org/10.1016/j.gca.2013.01.037

711   Magenheim, A.J., Spivack, A.J., Michael, P.J., Gieskes, J.M., 1995. Chlorine stable isotope

712   composition of the oceanic crust: Implications for Earth's distribution of chlorine. Earth Planet.

713   Sci. Lett. 131, 427–432. https://doi.org/10.1016/0012-821X(95)00017-7

714   Manzini, M., Bouvier, A.S., Baumgartner, L.P., Müntener, O., Rose-Koga, E.F., Schiano, P., Escrig,

715   S., Meibom, A., Shimizu, N., 2017. Weekly to monthly time scale of melt inclusion entrapment

716   prior to eruption recorded by phosphorus distribution in olivine from mid-ocean ridges. Geology

717   45, 1059–1062. https://doi.org/10.1130/G39463.1

718   Mattey, D., Lowry, D., Macpherson, C., 1994. Oxygen isotope compositions of mantle peridotite.

719   Earth Planet. Sci. Lett. 128, 231–241.

720   Matthews, A., Stolper, E.M., Eiler, Epstein, S., 1998. Oxygen isotope fractionation among melts,

721   minerals and rocks. Goldschmidt Conf. Toulouse 971–972.

722   McDonough, W.F., Sun, S. -s., 1995. The composition of the Earth. Chem. Geol. 120, 223–253.

723   https://doi.org/10.1016/0009-2541(94)00140-4

724   McKenzie, D.P., 1984. The generation and compaction of partial melts. J. Petrol. 25, 713–765.

725   https://doi.org/https://doi.org/10.1093/petrology/25.3.713

726   Moore, L.R., Gazel, E., Tuohy, R., Lloyd, A.S., Esposito, R., Steele-MacInnis, M., Hauri, E.H.,

727   Wallace, P.J., Plank, T., Bodnar, R.J., 2015. Bubbles matter: An assessment of the contribution

728   of vapor bubbles to melt inclusion volatile budgets. Am. Mineral. 100, 806–823.

729   Naumov, V.B., Dorofeeva, V.A., Girnis, A. V., Yarmolyuk, V. V., 2014. Comparison of major,

730   volatile, and trace element contents in the melts of mid-ocean ridges on the basis of data on

731   inclusions in minerals and quenched glasses of rocks. Geochemistry Int. 52, 347–364.

732   https://doi.org/10.1134/S0016702914050073

733   Nielsen, R.L., Sours-Page, R.E., Harpp, K.S., 2000. Role of a Cl-bearing flux in the origin of depleted

734   ocean floor magmas. Geochemistry, Geophys. Geosystems 1.

735   https://doi.org/10.1029/1999GC000017

736   Peres, P., Kita, N.T., Valley, J.W., Fernandes, F., Schuhmacher, M., 2013. New sample holder

737   geometry for high precision isotope analyses. Surf. Interface Anal. 45, 553–556.

738   https://doi.org/10.1002/sia.5061

739   Portnyagin, M., Almeev, R., Matveev, S., Holtz, F., 2008. Experimental evidence for rapid water

740   exchange between melt inclusions in olivine and host magma. Earth Planet. Sci. Lett. 272, 541–

741   552. https://doi.org/10.1016/j.epsl.2008.05.020

742   Schiano, P., 2003. Primitive mantle magmas recorded as silicate melt inclusions in igneous minerals.

743   Earth-Science Rev. 63, 121–144. https://doi.org/10.1016/S0012-8252(03)00034-5

744   Schilling, J.G., Zajac, M., Evans, R., Johnston, T., White, W., Devine, J.D., Kingsley, R., 1983.

745   Petrologic and geochemical variations along the Mid-Atlantic Ridge from 29 degrees N to 73

746   degrees N. Am. J. Sci. 283, 510–586. https://doi.org/10.2475/ajs.283.6.510

747   Seitz, S., Baumgartner, L.P., Bouvier, A.S., Putlitz, B., Vennemann, T., 2017. Quartz Reference

748   Materials for Oxygen Isotope Analysis by SIMS. Geostand. Geoanalytical Res. 41, 69–75.

749   https://doi.org/10.1111/ggr.12133

750   Shimizu, N., 1998. The geochemistry of olivine-hosted melt inclusions in a FAMOUS basalt ALV

751   519-4-1. Phys. Earth Planet. Inter. 107, 183–201. https://doi.org/10.1016/S0031-9201(97)00133-

752   7

753   Sobolev, A. V., Shimizu, N., 1993. Ultra-depleted primary melt in an olivine fron the Mid-Atlantic

754   Ridge. Nature 363, 151–154.

755   Stakes, D.S., 1991. Oxygen and hydrogen isotope compositions of oceanic plutonic rocks: High-

756   temperature deformation and metamorphism of oceanic layer 3. Stable Isot. Geochemistry A

757   Tribut. to Samuel Epstein 77–90.

758   Tormey, D.R., Grove, T.L., Bryan, W.B., 1987. Experimental petrology of N-MORB near the Kane

759   Fracture Zone: 22-25°N, mid-Atlantic ridge. Contrib. Miner. Pet. 96, 121–139.

760   Van Orman, J.A., Grove, T.L., Shimizu, N., 2002. Diffusive fractionation of trace elements during

761   production and transport of melt in Earth's upper mantle. Earth Planet. Sci. Lett. 198, 93–112.

762   https://doi.org/10.1016/S0012-821X(02)00492-2

763   Wallace, P., Carmichael, I.S.E., 1992. Sulfur in basaltic magmas. Geochim. Cosmochim. Acta 56,

764   1863–1874. https://doi.org/10.1016/0016-7037(92)90316-B

765 Watson, E.B., Müller, T., 2009. Non-equilibrium isotopic and elemental fractionation during

766   diffusion-controlled crystal growth under static and dynamic conditions. Chem. Geol. 267, 111–

767   124. https://doi.org/10.1016/j.chemgeo.2008.10.036

768 Zhang, Y., Ni, H., 2010. Diffusion of H, C, and O Components in Silicate Melts, in: Reviews in

769   Mineralogy and Geochemistry. Mineralogical Society of America, pp. 171–225.

770   https://doi.org/10.2138/rmg.2010.72.5

771 Zindler, A., Hart, S.R., Frey, F.A., Jakobsson, S.P., 1979. Nd and Sr isotope ratios and rare earth

772   element abundances in Reykjanes Peninsula basalts evidence for mantle heterogeneity beneath

773   Iceland. Earth Planet. Sci. Lett. 45, 249–262. https://doi.org/10.1016/0012-821X(79)90127-4

774

775

776

777 **Supplementary material:**

778 **Figure DR1**: Calibration line for IMF correction for oxygen isotope analyses in glasses and

779 olivine.

780 **Figure DR2**: P-elemental X-ray map of the ARP73-10-03_16 olivine

781 **Table DR1:** SIMS conditions

782 **Table DR2:** Major, trace, volatile, elements and $\delta^{18}O$ composition of melt inclusions

783 **Table DR3:** Oxygen isotopes in olivines

784